

On the possibility to detect the bound state of the Heisenberg ferromagnetic chain at intermediate temperature

Mithilesh Nayak¹ and Frédéric Mila¹

¹*Institute of Physics, Ecole Polytechnique Fédérale de Lausanne (EPFL), CH-1015 Lausanne, Switzerland*

(Dated: June 5, 2022)

Motivated by the lack of direct evidence with inelastic neutron scattering of the well documented bound state of Heisenberg ferromagnets, we use the time-dependent Thermal Density Matrix Renormalization Group algorithm to study the temperature dependence of the dynamical spin structure factor of Heisenberg ferromagnetic spin chains. For spin-1/2, we show that the bound state appears as a well defined excitation with significant spectral weight in the temperature range $J/10 \lesssim T \lesssim J/4$, pointing to the possibility of detecting it with inelastic neutron scattering near $k = \pi$ provided the temperature is neither too low nor too high - at low temperature, the spectral weight only grows as $T^{3/2}$, and at high temperature the bound state peak merges with the two-magnon continuum. For spin-1, the situation is more subtle because the bound state with two neighboring spin flips competes with an anti-bound state with two spin-flips on the same site. As a consequence, the relative spectral weight of the bound state is smaller than for spin-1/2, and a weak resonance due to the anti-bound state appears in the continuum. A clearer signature of the bound state (resp. anti-bound state) can be obtained if a negative (resp. positive) biquadratic interaction is present.

I. INTRODUCTION

The first evidence of bound states of spin waves in ferromagnets goes back to 1931 and Bethe's solution of the spin-1/2 Heisenberg chain[1], only one year after Bloch's theory of spin waves[2]. Since the Heisenberg ferromagnet conserves the number of spin-deviations and the states with different spin deviations are orthogonal to each other, Bloch realised that the low lying excitations are better understood in terms of spin-deviations, and that the Heisenberg model can be simply diagonalised in the subspace of single spin-deviation states in momentum basis, leading to the concept of spin-waves[2]. Similarly, the model can be studied in the subspace of two spin-deviation states, and the problem can be reduced to a one particle problem in the centre-of-mass momentum basis, with quite generally a continuum of two-magnon excitations and a well separated bound state emerging from two neighboring deviations[1, 3–7]. In 1D, the bound state exists as a separate excitation for all values of the wave-vector k .

The Heisenberg ferromagnet is realised in nature for instance in the spin-1/2 compound $(\text{C}_6\text{D}_{11}\text{ND}_3)\text{CuBr}_3$ or in the spin-1 compounds in CsNiF_3 or NiNb_2O_6 , to cite a few [8–12]. Inelastic neutron scattering (INS) experiments have probed spin-wave excitation by measuring the differential scattering cross-section in these ferromagnetic compounds[10, 13]. However, detecting the bound state of spin-waves in a ferromagnet has remained a challenge because INS measures single spin-flip excitations. At low temperatures the thermal ensemble is predominantly populated by fully aligned states, and accordingly one observes spin-wave excitations only. However, upon increasing the temperature, the thermal ensemble is populated with single spin deviation states and a spin-flip in these states would result in states in the two-spin devi-

ation subspace. Thus, INS experiments are in principle able to capture the bound-state of ferromagnets if they are performed at a strictly positive temperature.

There have been previous attempts to observe the bound states of spin-waves. Silberglitt and Harris have demonstrated that the bound states, in a 3D ferromagnet, have observable signatures in the thermal dynamical structure factor (DSF) in the large wavelength limit ($k = 0$)[14, 15]. The resonance of the bound state with the two-spin-wave continuum results in a broadening of the line width and an increase of the intensity of the single spin-wave peak which, a priori, can be detected in INS experiments. However, although the bound states of 3D ferromagnets exist as separate modes above a certain threshold of k , they are expected to gather a very small spectral weight compared to the main spin-wave excitation. Moreover, they lie too close to each other in energy to be properly resolved after thermal broadening of the respective peaks [15]. Thus, a direct detection of bound state in INS experiments could be difficult. Instead far-infrared transmission techniques have been used to find indirect signatures, and ferromagnetic resonances have been observed for $\text{CoCl}_2 \cdot 2\text{H}_2\text{O}(\text{CC2})$ [16, 17]. However, one cannot completely distinguish the bound state as the far infrared measurements are close to $k = 0$ where the bound state is not well-resolved from the single spin-wave excitation. To the best of our knowledge, a direct detection of the bound state of spin-waves in a Heisenberg ferromagnetic chain has not been achieved so far.

In the case of 1D ferromagnets the difference in excitation energy between the continuum and the bound state is largest at $k = \pi$, and this difference is larger than in its 3D counterpart. Therefore, a finite temperature INS experiment has a better chance to resolve and detect the bound state of spin-waves in 1D. To check this expectation, we directly simulate the DSF using finite temperature time dependent Density Matrix Renormal-

ization Group algorithm (henceforth referred to as thermal t-DMRG algorithm). We find the bound state of the spin-waves and compare its spectral intensity with that of the single spin-wave peak. Although bound states exist for ferromagnets with arbitrary spin, we focus our investigation to the finite temperature dynamics of spin-1/2 and spin-1 ferromagnetic chains in this paper.

The paper is organised as follows: in section II, we briefly describe the numerical method we used to obtain the results. In section III, we discuss the thermodynamics of the spin-1/2 FM chain obtained from thermal DMRG simulations and benchmark it with Wang-Landau Quantum Monte Carlo (QMC) algorithm from ALPS package. We then report on the finite temperature dynamics of spin-waves for the spin-1/2 FM chain. In order to characterise the bound state, we measure the spectral weights associated with it in the isotropic case and give simple arguments to motivate the shape of the spectral peak and the nature its temperature dependence which we support with spin-wave calculations done in the limit of vanishing magnetic field in Appendix B. In section IV, we extend the discussion to spin-1 chains. We discuss the remnants of resonances observed in the finite temperature DSF simulation of spin-1 FM chain using the dynamical quadrupolar structure factor at zero temperature, and we show that they come from anti-bound states and bound states that can be clearly identified when bi-quadratic interactions are included.

II. THE METHOD

INS experiments measure a differential scattering cross-section which is directly proportional to the dynamical structure factor (DSF) defined as the Fourier transform of time-dependent correlation functions:

$$C^{\alpha\bar{\alpha}}(l, t; \beta) = \text{Tr}[\hat{\rho}_{\beta} S^{\alpha}(\Delta r_l; t) S^{\bar{\alpha}}(0; 0)]$$

$$S^{\alpha\bar{\alpha}}(k, \omega)_{\beta} = \frac{1}{L^2} \int_{-\infty}^{\infty} dt \sum_l e^{-i(k\Delta r_l + \omega t)} C^{\alpha\bar{\alpha}}(l, t; \beta)$$

The computation of the DSF at finite temperature can be performed by using a time-dependent DMRG algorithm on a thermal ensemble (denoted as $\hat{\rho}_{\beta}$) pioneered by Barthel et al [18, 19] and Kestn et al [20]. The thermal ensemble is a mixed state and the matrix product density operator (MPDO) ansatz is better suited for simulating mixed states. However, it is more convenient to construct the MPDO in terms of purified matrix product states (MPS). A purified MPS is defined on an enlarged Hilbert space, namely a physical Hilbert space and an ancillary Hilbert space [21–23]. We simulate purified states up to half the inverse temperature denoted as $\hat{\rho}_{\beta/2}$ by applying the time evolution operator in second-order Suzuki-Trotter steps [24] and then compute the ensemble average of observables by tracing over the ancillary degrees of freedom. Since the thermal ensemble is Hermitian (i.e. $\hat{\rho}_{\beta/2} = \hat{\rho}_{\beta/2}^{\dagger}$), we can write the follow-

ing expression for computing observables $\text{Tr}(\hat{\rho}_{\beta/2}^{\dagger} O \hat{\rho}_{\beta/2})$. By only tracing over ancillary degrees of freedom, i.e. $\text{Tr}_a(\hat{\rho}_{\beta/2}^{\dagger} \hat{\rho}_{\beta/2})$, we obtain the full thermal ensemble ($\hat{\rho}_{\beta}$) as a MPDO. This approach of constructing the MPDO ensures its complete positiveness.

The computation of the thermal DSF essentially consists of two steps: (i) One simulates the thermal ensemble by performing imaginary time evolution; (ii) One simulates real time evolution after applying the relevant spin operator to the thermal ensemble. For the simulation of the thermal ensemble, we kept our imaginary time evolution trotter steps to be $\Delta\beta = 0.01/J$ keeping the truncation weights to be $\mathcal{O}(10^{-8})$ and for real-time evolution we kept the trotter steps to be $\Delta t = 0.1/J$ keeping the truncation weights to be $\mathcal{O}(10^{-4})$. We compute the time-dependent correlation functions as follows:

$$C^{\alpha\bar{\alpha}}(l, t; \beta) = \text{Tr}[\hat{\rho}_{\beta/2}^{\dagger} e^{iHt} S^{\alpha}(\Delta r_l; 0) e^{-iHt} S^{\bar{\alpha}}(0; 0) \hat{\rho}_{\beta/2}]$$

$$= \text{Tr}[\hat{\rho}_{\beta/2}^{\dagger} S^{\alpha}(\Delta r_l; 0) e^{-iHt} S^{\bar{\alpha}}(0; 0) \hat{\rho}_{\beta/2} e^{iHt}]$$

Since the spatial Fourier-transformed correlations in *positive* and *negative* times are related to each other by conjugation, we simulate only the positive time correlations and extract the case for negative times from them. We simulate up to a final time $t_f = 20/J$ (instead of infinite time) to obtain the DSF, which is large compared to the interaction strength ($1/J$). We also made sure that, for all the system sizes, the temporal spread of correlations does not reach the boundary. Upon taking the temporal Fourier transform, the DSF gets convoluted with a sharp window of finite time which results in numerical artefacts. To overcome this problem, the time-dependent correlation function is allowed to exponentially decay to 0 at infinite times by multiplying the correlations with a gaussian filter. We chose $2(\pi t_f^2)^{-1/2} e^{-4t^2/t_f^2}$ in order to smooth out the finite time effects [24, 25]. The resulting numerical DSF has a spatial resolution of $\Delta k = 2\pi/L$ and a frequency resolution of $\Delta\omega = \pi/t_f$.

Numerically, the spin-1 chain poses a separate challenge. Since the physical dimension increases and the complexity of the code scales as $\mathcal{O}(d^6\chi^3)$, it is expensive in computational resources. We restricted ourselves to 60 sites and $\chi = 400$ for the thermal DSF computations. For larger number of sites, one would have to keep a larger bond-dimension in order to faithfully represent the thermal ensemble. In order to avoid the boundary effects from the time-evolution cone touching the sides of the chain, we limit ourselves to final time $t_f = 14/J$. This reduces our frequency and spatial resolution as compared to the spin-1/2 chain. Since we work with a small chain size and a small final time evolution, we applied a gaussian filter $2(\pi t_f^2)^{-1/2} e^{-4t^2/t_f^2} e^{-4x^2/(L-1)}$ to the DSF in order to smoothen out both temporal and spatial finite size effects.

III. SPIN-1/2 FERROMAGNETIC CHAIN

A. Model, scattering states, and bound state

We discuss the spin-1/2 ferromagnetic Heisenberg chain with L sites and periodic boundary conditions described by the Hamiltonian:

$$\mathcal{H}_{FM} = -J \sum_{i=1}^L \mathbf{S}_i \cdot \mathbf{S}_{i+1}, \quad J > 0 \quad (1)$$

The low-lying excitations can be described in terms of spin-deviations.

1. The ground state can be chosen to be the state which is fully-aligned in a given direction. It has no spin-deviation. The ground state energy is $E_0 = -JL/4$.
2. There are L one-spin-deviation states. The Hamiltonian is trivially diagonalized in the momentum basis, leading to spin-wave states with energy:

$$\omega_1(k) = E_1(k) - E_0 = J(1 - \cos k) \quad (2)$$

3. There are $L(L-1)/2$ two-spin deviation states which can be written in the basis of the centre of mass momenta. One can classify them into two kinds of states: (i) $L(L-3)/2$ scattering states of pairs of spin-waves, and (ii) L bound states of spin-waves. The energy of the scattering states is given by the sum of the energies of two spin-waves:

$$\begin{aligned} \omega_2(K, p) &= J(1 - \cos k_1) + J(1 - \cos k_2) \\ &= 2J \left(1 - \cos \frac{K}{2} \cos p \right) \end{aligned} \quad (3)$$

In the last line, we used the centre of mass momentum $K \equiv k_1 + k_2$ and the relative momentum $p \equiv (k_1 - k_2)/2$. The bound-state energy can be derived by following the Green's function approach [4] or simply solving the eigenvalue equation [5, 26] (see Appendix A for details). The dispersion relation of the bound state is:

$$\omega_{2,BS}(K) = E_{2,BS}(K) - E_0 = J \sin^2 \frac{K}{2} \quad (4)$$

The bound state exists as a mode separated from the continuum of two spin-waves. The difference between the lower boundary of the continuum (given by $p = 0$ in Eq.3) and the bound state energy is given by:

$$4J \sin^2 \frac{K}{4} - J \sin^2 \frac{K}{2} = 4J \sin^4 \frac{K}{4} \geq 0,$$

with the equality holding only for $K = 0$. Thus, the bound state energy lies below the two-spin-wave continuum and only meets it at $K = 0$.

B. Thermodynamics

In order to benchmark the first step of the computation of the thermal DSF, we simulate the thermodynamics of the spin-1/2 FM chain. Bloch discussed the low-temperature thermodynamics of 3D ferromagnets in terms of non-interacting spin-waves [2]. Since the density of spin-waves in the model is very small at low-temperatures, the spin-waves can be assumed to be non-interacting. This leads to the well known temperature dependence of the magnetisation $M(T) \sim M(0) \left(1 - (T/T_c)^{\frac{3}{2}} \right)$ for 3D. If one tries to extend this argument to 1D, one gets a diverging correction to the magnetization. However, from Mermin-Wagner-Hohenberg theorem, the magnetisation of the 1D ferromagnet should be zero. Therefore, Takahashi complemented the non-interacting spin-wave theory with a constraint of zero magnetisation [27], a method known as modified spin-wave theory, to explain the low temperature thermodynamics of the 1D ferromagnet. This leads to the following low-temperature expansion of the free energy of the 1D ferromagnet:

$$\begin{aligned} F &= \frac{E_0}{L} - \frac{\zeta\left(\frac{3}{2}\right)}{\sqrt{2\pi}} T^{\frac{3}{2}} + T^2 \\ &+ \sqrt{\frac{2}{\pi}} \left(\zeta\left(\frac{1}{2}\right) - \frac{\zeta\left(\frac{5}{2}\right)}{16} \right) T^{\frac{5}{2}} + \mathcal{O}(T^3) \end{aligned} \quad (5)$$

where, $\zeta(\alpha)$ is the Riemann-zeta function. Other interesting thermodynamic quantities such as the entropy, the average energy and the specific heat can be extracted by using statistical physics relations, leading to the low temperature behaviours

$$\begin{aligned} S &\propto T^{\frac{1}{2}} \\ \langle E \rangle - E_0 &\propto T^{\frac{3}{2}} \\ C_v &\propto T^{\frac{1}{2}} \end{aligned}$$

Note that the free energy of the 1D Ferromagnet has also been computed using thermal Bethe-Ansatz by Takahashi [28]. The thermal Bethe-Ansatz leads to a set of coupled integral equations on spin-deviations which is analytically solvable in the limit of very low temperature. The agreement between the modified spin-wave theory and the thermal Bethe Ansatz results is excellent at very low temperature [27, 28].

Numerically, we have access to the thermal ensemble, so we determined the thermal ensemble energy per unit length for systems of $L = 60, 80, 100, 120, 140$ sites, and performed a $1/L$ finite size scaling of the data. We obtained the specific heat per unit length from it by numerically differentiating with respect to temperature. We then numerically integrated the specific heat to compute the entropy per unit length, assuming the entropy of FM chain at $T=0$ to be 0. The results for the energy and the entropy lead us to the estimation of the free energy. This

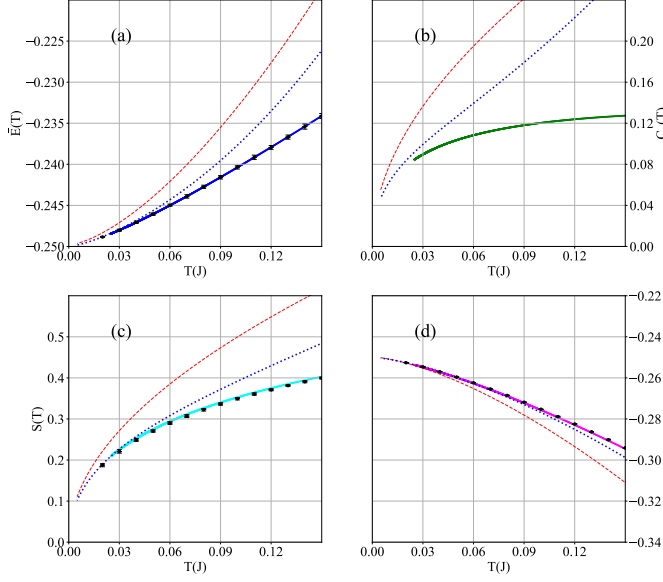


FIG. 1: Thermodynamics of the spin-1/2 FM Heisenberg chain. The solid lines stand for our thermal DMRG data. The non-interacting spin-wave thermodynamic quantities are shown as red dashed line while the modified spin-wave thermodynamic quantities (low temperature expansion in Eq. 5) are shown as blue dotted lines. The black symbols are QMC data obtained with the Wang-Landau algorithm. See main text for details.

sequence of steps is summarized below:

- (i) $\langle E \rangle_\beta = \frac{1}{LZ} \text{Tr} [\mathcal{H} e^{-\beta \mathcal{H}}] = \frac{1}{L} \text{Tr} [\hat{\rho}_{\beta/2} \mathcal{H} \hat{\rho}_{\beta/2}]$
- (ii) $C_v(\beta) = \frac{d}{dT} \langle E \rangle_\beta$
- (iii) $S(\beta) = k_B \int_\infty^\beta \frac{C_v(\beta)}{\beta} d\beta$
- (iv) $F(\beta) = \langle E \rangle_\beta - TS(\beta)$

We find good agreement of the numerics with modified spin-wave theory for low temperature, where non-interacting spin-waves dictate the thermodynamics (see Fig. 1). The disagreement in the free-energy density of the modified spin-wave theory might be addressed by thermal Bethe-Ansatz where the thermal statistics is determined in terms of spin-deviations (which includes interactions between spin-waves automatically), but this is beyond the scope of this article. To benchmark our results at not so low temperatures, we have used the Wang-Landau QMC code of the ALPS package's to calculate these thermodynamic quantities [29–31] using $L = 140$ sites, a cut-off $\Lambda = 10^4$, and a temperature step $\Delta T = 10^{-3}(1/J)$. The agreement with our determination of the free-energy, ensemble energy and entropy is perfect

within the error bars of the QMC data.

C. Finite-temperature dynamics

Since the scattering neutron can flip one spin in the chain, it connects the existing state with another state with an extra spin deviation. So we now explore the consequences of the extra spin deviations in the thermal ensemble of the spin-1/2 FM chain. Flipping one spin in the single spin-deviation state of the system leads to two possibilities - it either returns to the FM ground state or creates an additional spin-deviation, resulting in a two-spin-wave state or a bound state. Since finite temperature results in a finite population of single-spin deviation states, the thermal DSF can detect the bound state. However, in the higher temperature ranges, the thermal broadening of spin-wave excitations assisted by the two-magnon processes obscures the bound state. Therefore, in order to detect the bound states, one might aim for a temperature range where FM chain can develop an appropriate thermal population of single spin-deviation states such that the bound state has observable spectral intensity while at the same time the thermal broadening of the spin-wave excitation does not cloak the bound state. Since the model is isotropic, the transverse (S^{+-}) and longitudinal component (S^{zz}) of the DSF are essentially the same up to a multiplicative factor. We show the longitudinal component in Fig. 2 but the same discussion carries over to transverse components. The bound state is detectable as a separate mode from spin-wave excitation in the range of temperatures from $J/10$ to $J/4$ not too far from $k = \pi$).

We note that there is thermal spectral weight in the negative ω regime, which is due to the de-excitation of a spin-wave state to the fully aligned state. Consider n_B as the occupancy factor of spin-waves in the lattice, then the spectral peak associated with the excitation of a fully aligned state to a spin-wave state is proportional to $n_B + 1$, while a de-excitation would be proportional to n_B . This implies that the spectral weight for the process corresponding to a spin-wave de-excitation is $n_B/(n_B + 1) = e^{-\beta \omega_1(k)}$ times the spectral weight due to a spin-wave excitation. Because of the exponential decay with respect to the wave vector k , spectral weight can only be observed close to $k = 0$ for de-excitation processes.

Next, we characterise the thermal spectral weight of the bound state in the section cut $k = \pi$ numerically. We computed the area under the curve for the bound state (I_{BS}) and for spin-wave excitations (I_{SW}) at $k = \pi$ obtained by integrating the longitudinal DSF over different frequency ranges (Fig. 3a):

$$I_{BS}(k = \pi; \beta) = \int_{\omega_1}^{\omega_2} S^{zz}(k = \pi, \omega)_\beta d\omega$$

$$I_{SW}(k = \pi; \beta) = \int_{\omega_2}^{\omega_3} S^{zz}(k = \pi, \omega)_\beta d\omega,$$

where we choose ω_1 and ω_3 such that the section-cut

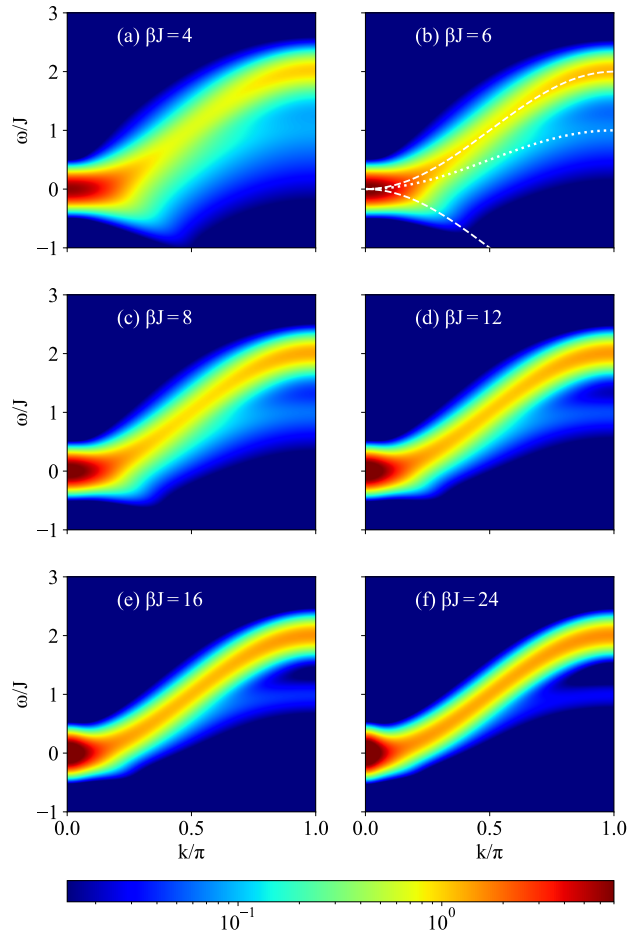


FIG. 2: Longitudinal thermal DSF ($S^{zz}(k, \omega)_\beta$) of the spin-1/2 FM chain with $L = 140$ sites, $\chi = 400$ and $t_f = 20/J$. Since the system is isotropic, the spin-flip DSF component ($S^{xx}(k, \omega)_\beta$) is equal to the longitudinal DSF component. As the temperature is lowered (or the inverse temperature β increased), the bound state progressively loses spectral weight. The features in Fig. 2a) are consistent with the spin-wave and bound state dispersion relations of Eq.2 and Eq.4.

curve lies below 10^{-4} outside this range, while ω_2 is the value where the section cut curve reaches a local minimum between the bound state peak and the main spin-wave excitation peak. The results for $L = 60, 80, 100, 120$, and 140 have been extrapolated in $1/L$ to the thermodynamic limit. A log-log plot of these extrapolated areas is shown in Fig. 3b. It is difficult to push the thermal DMRG algorithm to the $T = 0$ limit since one has to simulate up to $\beta J = \infty$. However, for $T = 0$, the DSF should capture only the spin-wave excitation, so the area under the bound state curve is $I_{BS}(k = \pi; \beta = \infty) = 0$. We determined the area under the main spin-wave excitation at $T = 0$ by ensuring that the sum of the area of the

spin-wave peak and of the bound state peak is constant. We make the following observations at this section-cut : (a) The spectral peak of the bound state is asymmetric around its maximum and has a longer tail extended to low energy.

(b) The area under the spectral peak associated with the bound state scales with temperature as $T^{3/2}$.

The DSF measures the spectral signature at coordinates corresponding to the difference of momenta and energies between the initial and final states. The asymmetry in the spectral peak of the bound state can then be explained by considering the process of two spin-waves with momentum p and momentum π contributing to the thermal weight of bound state at momentum $K = \pi + p$ whose thermal DSF signature is then observed at $k = K - p = \pi$. The thermal population of the single spin-wave states with smaller momentum p is higher, so a spin-deviation on these states will result in a larger spectral weight. The spectral signals in the DSF are observed at $\omega = \Delta E(p) = \omega_{BS}(\pi + p) - \omega_1(p)$. Since $\Delta E(0) = J$, we have the spectral peak at $\omega = J$ but as we increase p we find the thermal population decreasing and hence a long tail of spectral weight to negative ω is seen. The temperature dependence of the spectral weights is also deduced from the above discussion- the majority of the thermal spectral weight is due to the thermal population of single spin-waves near $k \approx 0$ which goes as $T^{3/2}$. This is indeed the leading behaviour of the area under the curve for the bound state. Similarly, it implies that the decrease in the spectral weight of the main spin-wave excitation would indeed have the same temperature dependence. We verified this from by plotting the following quantity (inset of Fig. 3b)

$$\Delta I_{SW}(k = \pi; \beta) = I_{SW}(k = \pi; \infty) - I_{SW}(k = \pi; \beta)$$

These explanations can be qualitatively supported by simple considerations (see Appendix B).

Finally, in Fig. 4, we present the section-cuts of the longitudinal component of the thermal DSF at various wave-vectors. As the wave-vector increases towards π , we find that the bound state mode is completely separated for low enough temperatures. It is interesting to note that for $k = 0.6\pi$ and $k = 0.7\pi$, the bound state is not completely separated from the two-magnon continuum. The presence of the bound state appears as an asymmetric spectral peak with a long tail.

IV. SPIN-1 FERROMAGNETIC CHAIN

A. Heisenberg model

We can extend the analysis of the spin-1/2 chain to the spin-1 ferromagnetic Heisenberg chain. The dispersion relation for a spin-wave excitation in the chain is $2J(1 - \cos k)$, where J is the interaction strength. For the two spin-deviation subspace, we have two types of

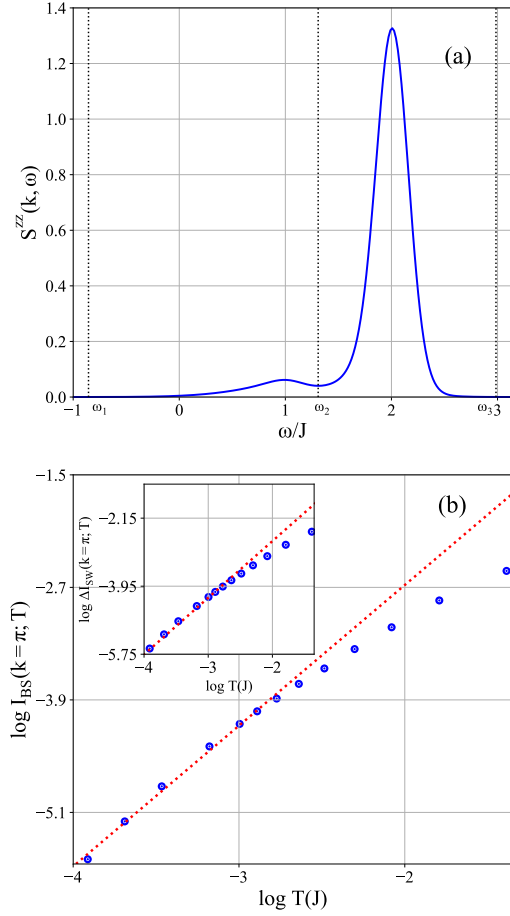


FIG. 3: (a) Numerical longitudinal thermal DSF section cut of the spin-1/2 FM chain at $k = \pi$ and $\beta J = 8$. The spin-wave excitation is the main spectral peak at $\omega = 2J$ and the bound state is the smaller spectral peak at $\omega = J$; (b) log-log plot of the area under the boundstate versus temperature (see main text for details). At low temperatures, it is consistent with an exponent $3/2$ (red dotted line). Inset: log-log plot of the difference between the area under the main spin-wave excitation at zero temperature and finite temperature versus temperature. At low temperature, it is also consistent with an exponent $3/2$ (red dotted line).

solutions: the two spin-wave scattering states and the bound state. The bound state solution can be determined by setting up the transfer matrix equation, as in the spin-1/2 case (see appendix A) and by looking for the *localized* solution [4–7, 32]. In the thermodynamic limit, the dispersion relation of the bound state in the spin-1

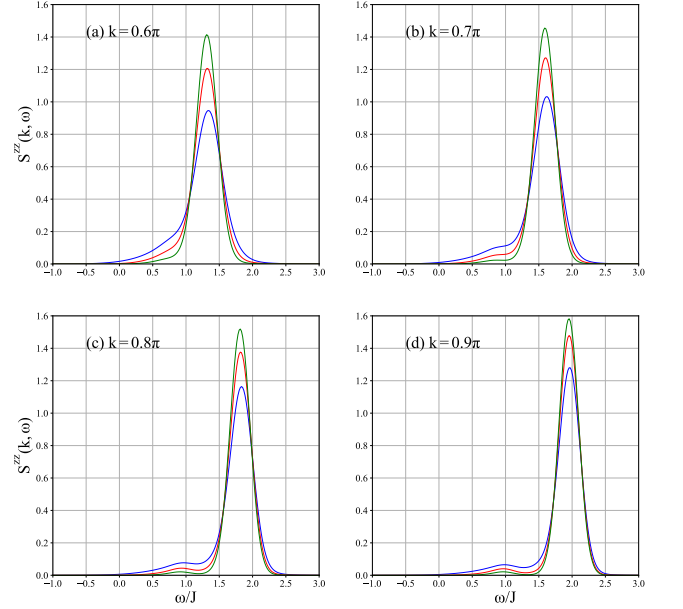


FIG. 4: Comparison of section cuts of the longitudinal thermal DSF of the spin-1/2 FM chain with 140 sites for $\beta J = 8$ (blue), $\beta J = 16$ (red) and $\beta J = 32$ (green). As the temperature decreases, the spectral peak associated with the bound state decreases in height and gets separated from the single spin-wave excitation, but for section-cuts at $k = 0.6\pi$ (shown in a) and $k = 0.7\pi$ (shown in b), the bound state is not completely separated even at very low temperatures.

chain is given by:

$$\omega_{2,BS}(k) = \frac{11J}{3} + \frac{J}{3} \left(\frac{13 + 12 \cos k}{x} + x \right)$$

with

$$x^3 = -100 - 126 \cos k - 27 \cos 2k + 12\sqrt{6} \sqrt{\left(\cos \frac{k}{2} \right)^6 (29 + 27 \cos k)}$$

The bound state, like in the spin-1/2 FM chain, exists as a separate mode and lies below the two-spin-wave continuum except at $k = 0$.

Similar to spin-1/2 FM chain, we can also expect to experimentally detect the bound state in a spin-1 FM chain at finite temperature. And indeed, the numerical simulations of the thermal DSF clearly show the presence of a bound state. The energy difference between the single spin-wave excitation and the bound state of spin-waves is maximum at $k = \pi$, like in the spin-1/2 chain. Thus, with an energy difference of J , one can resolve the peak associated with bound state and the peak associated with the main spin-wave excitation at $k = \pi$. In the infrared-limit,

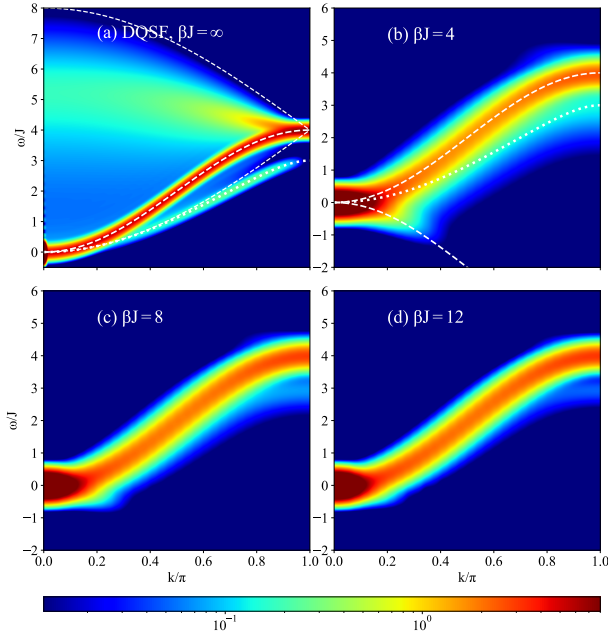


FIG. 5: Comparison of (a) the two-spin-deviation spectrum observed in Dynamical Quadrupolar Structure Factor (DQSF) with (b) the thermal DSF of the spin-1 FM chain. (c) and (d) show the thermal DSF at different finite temperatures. The DQSF has been computed on $L = 240$ sites and a final time evolution of $t_f = 24/J$. The thermal DSF simulation has been carried out with $L = 60$ and $t_f = 14/J$. As compared to the spin-1/2 chain, the resolution of the modes is smaller in the case of the spin-1 chain. In the DQSF and thermal DSF, the dashed lines show the spin-wave excitation, while the dotted white line shows the bound state.

even though the bound state only touches the spin-wave continuum at $k = 0$, the bound state feature is cloaked because of the thermal broadening of the single spin-wave excitation and of two-spin-wave processes.

The first point of difference between spin-1/2 and spin 1 FM chains is that the main spin-wave excitation spectral peak is twice as large for the spin-1 chain as compared to the spin-1/2 chain (see Fig. 6). At the same time, the spectral peak corresponding to the bound state is of the same height for both cases. Therefore, the relative intensity of the bound state with respect to the main spin-wave is halved. Accordingly, detecting the bound state can be expected to be more challenging in spin-1 FM chains. In addition to this, in spin-1 FM chains, there are some remnant features of *resonances* in the two spin-wave continuum in the thermal DSF near $k = \pi$ (see Fig. 5b). The difference arises from the fact that, unlike the spin-1/2 FM chain, the spin-1 FM chain allows for two spin deviations on the same site. Therefore, exciting a spin deviation on the thermal population of single spin-wave state could lead to an anti-bound state when two spin-deviations are on the same site or to a bound state

when the two spin deviations are not on the same site. For the pure Heisenberg model, the energy of the anti-bound state lies within the two-spin-wave continuum [33] and this results in a resonance.

To better characterise the zero-temperature two-spin deviation spectrum, it is useful to look at the dynamical quadrupolar structure factor (DQSF). The quadrupolar structure factor has 3 equivalent components for an isotropic system corresponding to the change of on-site magnetisation (ΔS^z), namely - longitudinal component ($\Delta S^z = 0$), transverse component ($\Delta S^z = \pm 1$) and pairing component ($\Delta S^z = \pm 2$) [34]. We present the numerical results of the pairing component but we verified that the three components give the same spectral features up to a multiplicative factor. To be specific, the pairing component of the DQSF is defined by:

$$C_{Q,2}(i, j; t) = \frac{1}{2} \left[\langle (S^-(j; t))^2 (S^+(i))^2 \rangle + \text{h.c.} \right]$$

$$Q_2(k, \omega) = \frac{1}{L^2} \int_{-\infty}^{\infty} dt e^{i\omega t} \sum_{i,j} e^{-ik(r_j - r_i)} C_{Q,2}(i, j; t)$$

We find clear evidence of a resonance extending into the two-spin-wave continuum around $k = \pi$ (in Fig. 5a) which, at finite temperature, leads to the subtle features observed in the thermal DSF.

B. Bilinear-biquadratic model

In order to get more insight into the antibound state, we extend our model to include a nearest neighbour biquadratic coupling,

$$\mathcal{H}_{\text{BLBQ}} = J \sum_i \cos \theta (\mathbf{S}_i \cdot \mathbf{S}_{i+1}) + \sin \theta (\mathbf{S}_i \cdot \mathbf{S}_{i+1})^2$$

The ferromagnetic phase for this model is located in the interval $\theta \in (\pi/2, 5\pi/4)$. The spin-1 Heisenberg FM chain is recovered for $\theta = \pi$. We simulate the DQSF in the FM phase of the BLBQ model for $\theta \in (\pi/2, 3\pi/4]$ and, for θ not too large, we find clear evidence of an anti-bound state above the two-spin-wave continuum. Following the Green's function approach by Wortis, we found the same dispersion relations for the bound states and anti-bound states as has been obtained for this model by Aghahosseini et. al [35]. They agree with the numerical determination of the spectrum in Fig. 7. As we increase θ from $\pi/2$ towards the Heisenberg FM point, we find that the anti-bound state enters the continuum, explaining the presence of a resonance at the Heisenberg point. This is the feature whose subtle remnants can be observed in the thermal DSF. We find that a stronger biquadratic interaction leads to a well-separated anti-boundstate mode. Remarkably enough, as we decrease the biquadratic interaction in the range of $\theta \in [3\pi/4, 9\pi/10]$, we find either an anti-bound state or a bound state at a given k vector. This points to a three-way competition between

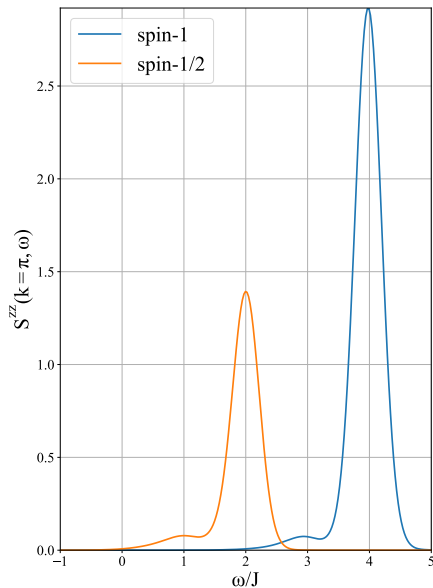


FIG. 6: Comparison between the thermal DSF section cut of the spin-1/2 and spin-1 FM Heisenberg chains at $k = \pi$ and $\beta J = 8$. In order to have an appropriate comparison we present here data obtained from keeping the same parameters for both chains, namely $L = 60$, $\chi = 400$ and $t_f = 14/J$. The height of the bound state peak is the same, but the peak corresponding to the spin-wave excitation is twice as large for spin -1 than for spin-1/2 chain.

anti-bound state, bound state and two-magnon scattering state when we introduce temperature.

The thermal DSF simulation of the spin-1 bilinear and biquadratic chain leads to the spectral signature of bound states and anti-bound states in the BLBQ chain shown in Fig. 8. We find that the anti-bound states lose most of the spectral weights as compared to the zero temperature simulation of the DQSF. The visible spectral weight lies close to the region $k \approx \pi$ for values of θ where the biquadratic coupling is large enough so that that the anti-bound state is separated from the continuum by a gap (Fig. 8a). The bound states are barely visible, even though they exist for $\theta \in [3\pi/4, \pi)$ (see Fig. 7), but as we decrease the temperature to the appropriate level for θ greater than π , we find that the bound state gathers enough weight to be distinguished from the main spin-wave excitation. Thus, a finite-temperature INS experiment could better observe the bound state in the presence of a significant negative biquadratic interaction. This is not the most generic situation in experimental realisations of spin-1 chains, but negative biquadratic interactions can be generated in the presence of a quasidegenerate orbitals [36].

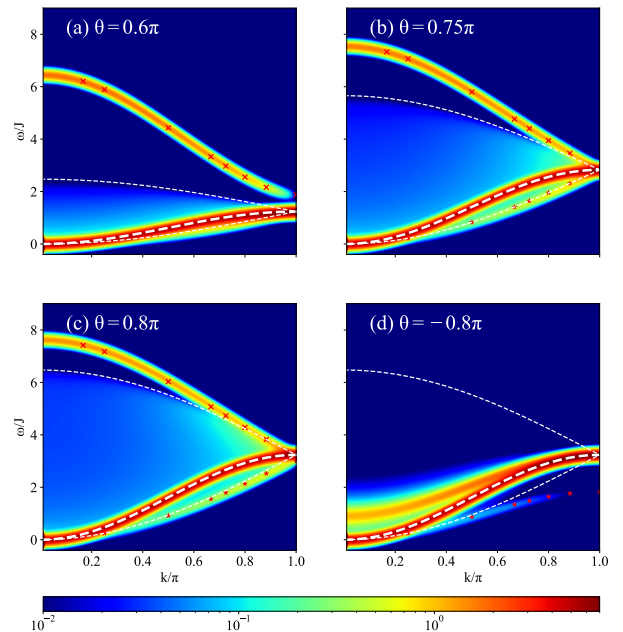


FIG. 7: DQSF plots for the spin-1 BLBQ model, $L = 240$, $t_f = 24/J$, $T = 0$. We find that the bound state (red stars) is more prominent as k goes to π , but for lower values of k it lies within the two-magnon continuum (bounded by the white dotted lines). By contrast, the anti-bound state (red crosses) is more prominent for lower values of k and in some cases merge with the two-magnon continuum for larger values of k . The white dashed lines indicate the single magnon dispersion.

V. CONCLUSION

The dynamics of multiple excitations in ferromagnets is very rich and it forms the bedrock to understand the antiferromagnetic case [1, 37–40]. Upon diagonalising the two-spin deviation subspace of the 1D Heisenberg ferromagnet one finds the presence of a bound state. The thermal DMRG simulations confirmed that the bound state can be detected when one thermally populates the spin-wave states. From finite temperature numerics, we noted the asymmetry of the bound state spectral peak and found that the spectral weight of the bound state increases with temperature as $T^{3/2}$. We gave a simple qualitative explanation for the former considering only contribution from prominent processes (i.e. excitations from fully aligned states and single spin deviation states).

INS experiments have already been conducted on ferromagnets, but at very low temperature (see e.g. Ref. [10], where the exchange coupling (J) was 66 K while the measurements have been made at temperatures below 4K ($\sim J/16$). This temperature regime was not ideal to observe the bound state because its spectral weight is about one-hundredth of that of the spin-wave excitation in this temperature range. With the improvements

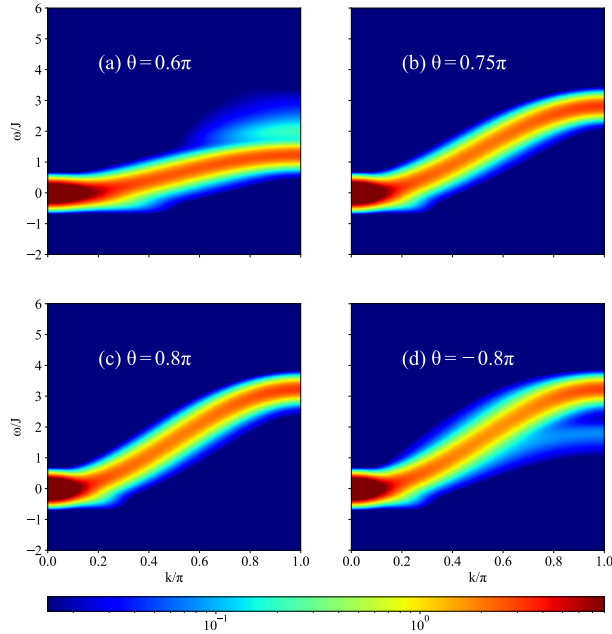


FIG. 8: Longitudinal thermal DSF ($S^{zz}(k, \omega)$) of the FM bilinear-biquadratic spin-1 chain with $L = 60$ and $T = J/10$, with $t_f = 16/J$. As the biquadratic coupling is decreased from (a) to (d), the clear signature of an anti-boundstate is replaced by that of a boundstate. Note that the anti-boundstate gathers very little spectral weight at finite temperature.

in neutron scattering technology and performing a scan for $k = \pi$ (where the separation between the spin-wave and the bound state is maximum) at a higher temperature regime ($J/10$ to $J/4$), we have shown that it should be possible to detect the bound state in ferromagnetic chains, the most favourable case being spin-1/2.

The same arguments can be extended to 2D and 3D Heisenberg ferromagnets where there are 2 bound states and 3 bound states at the edge of the Brillouin zones respectively. In contrast to 1D, in 2D ferromagnets, there is one bound state which enters the continuum, while the other bound state exists for all k . In 3D, the three bound states exist beyond certain threshold values of k close to the edge of the Brillouin zone. Thus, in higher dimensions, the bound states become difficult to detect directly. Studying the resonances when the bound state enters the continuum seems to be a more appropriate approach. Furthermore, the thermal broadening of the bound states and of the main spin-wave excitations are additional bottlenecks in higher dimensions.

Furthermore, for higher values of the spin, the ratio of the difference between the bound state and the spin-wave energies and the main spin-wave energy at $k = \pi$ decreases. Thus, after thermal broadening, the bound state and the spin-wave peaks may not be easily distinguishable. So the best candidate to observe the bound

state is the spin-1/2 FM chain.

Finally, in real materials, finite temperature induces both acoustic and optical phonon modes which could obscure the bound state spectral weights in the magnon energy spectrum observed in INS experiments [12, 41]. However, upon choosing a material with appropriate strength of magnetic exchange coupling, one should be able to separate the magnons from the phonons, especially at the edge of the Brillouin zone. Additionally, switching on the external magnetic field would decouple the spin degrees of freedom from the lattice vibrations and could lead to clear detection of the bound state.

In conclusion, we hope that the present paper will encourage specialists of inelastic neutron scattering to look for the bound state of the ferromagnetic chain, a ninety year old prediction still awaiting for a direct confirmation.

ACKNOWLEDGEMENTS

We are very grateful to Noam Kestlin for insightful discussions on the Thermal DMRG code, and to Henrik Rønnow for discussions regarding neutron scattering experiments. MN thanks Aubry Jaquier for helping in setting up the ALPS package. MN also thanks Olivier Gauthé and Jeanne Colbois for helpful discussions. The numerical simulations were performed on the SCITAS clusters at EPFL. We acknowledge the funding from Swiss National Science Foundation.

Appendix A: Two-spin deviation spectrum of spin-1/2 FM chain

As discussed in the main text, the two-spin-deviation subspace of the FM Heisenberg model has two types of solutions: (i) two-spin-wave scattering states and (ii) bound state of spin-waves. In this section, we discuss the form of bound state. One can consider a general state in the two-spin deviation subspace [5, 26, 42] as:

$$|2\rangle_{k_1, k_2} = \sum_{x_1 < x_2} a_{k_1, k_2}(x_1, x_2) S_{x_1}^+ S_{x_2}^+ |\text{GS}\rangle \quad (\text{A1})$$

where $a_{k_1, k_2}(x_1, x_2)$ is the coefficient dependent on the position of spin-deviations in the chain. One can assume the Bethe-Ansatz form of the solution, i.e. superposition of an incident wave and a scattered wave. One can work in centre of mass coordinates defined by

$$\begin{aligned} K &= k_1 + k_2, & R_{12} &= \frac{r_{x_1} + r_{x_2}}{2} \\ p &= \frac{k_1 - k_2}{2}, & r_{12} &= r_{x_1} - r_{x_2} \end{aligned}$$

to get the following results:

1. For the two-spin-wave scattering states, one can proceed to develop the eigenvalue equation and to

find the travelling solution

$$a_{K,p} \approx \frac{\sqrt{2}}{L} \cos[pr_{12} + \theta] e^{iKR_{12}}$$

where the definition of the phase factor θ is obtained from the boundary condition of the transfer matrix equation as follows:

$$\cot \theta = \frac{\sin p}{\cos \frac{K}{2} - \cos p}$$

2. For the bound state, one gets

$$a_{K,\tilde{p}}(x_1, x_2) = \frac{1}{2\sqrt{L}} \frac{|\sin \frac{K}{2}|}{\sqrt{1 - \cos \frac{K}{2}}} e^{iKR_{12}} e^{-\tilde{p}(|r_{12}| - 1)} \quad (\text{A2})$$

where, \tilde{p} is defined as

$$\tilde{p} = -\ln \cos \frac{K}{2}$$

Numerically, we determine the transverse dynamical structure factor of a spin-1/2 FM chain at zero temperature (i.e. $\beta \rightarrow \infty$) by evaluating Eq.1 with $\alpha = -$, $\tilde{\alpha} = +$. This leads to:

$$\begin{aligned} S^{-,+}(k, \omega) &= \frac{1}{L} \sum_{i,j} e^{-ik(r_j - r_i)} e^{i\omega t} \langle \text{GS} | S^-(j, t) S^+(i, 0) | \text{GS} \rangle \\ &= \frac{2\pi}{L} \delta(\omega - \omega_1(k)) \end{aligned} \quad (\text{A3})$$

So, in an INS experiment, one just observes the spin-wave excitation (shown in Fig.9a) whose dispersion relation $\omega_1(k)$ is given in Eq.2 of the main text.

To probe the two-spin deviation sector, it is convenient to study operators which leads to two-spin deviations in the FM ground state, and to use the time-dependent DMRG algorithm to compute the time-dependent correlation functions based on these operators.

One such operator and its conjugate are defined by:

$$\hat{O}_2^\pm(i) = S^\pm(i) S^\pm(i+1)$$

and the two-spin-deviation correlation function reads

$$C_2(i, j; t) = \frac{1}{2} \left[\langle \text{GS} | \hat{O}_2^-(j, t) \hat{O}_2^+(i, 0) | \text{GS} \rangle + \text{h.c.} \right]$$

We took the spatial and temporal Fourier transform to obtain the two-spin wave dynamical structure factor:

$$S_2(k, \omega) = \frac{1}{L^2} \int_{-\infty}^{\infty} dt \sum_{i,j} e^{-ik(r_j - r_i)} e^{i\omega t} C_2(i, j; t)$$

Our numerical evaluation of $S_2(k, \omega)$ clearly shows a two-spin wave continuum and a bound state of spin-waves, as shown in Fig. 9b. This confirms the structure of the two spin deviation subspace. However, we are not aware of any experimental technique in which a 2-spin-wave spectrum can be measured at very low temperatures for the spin chain compounds.

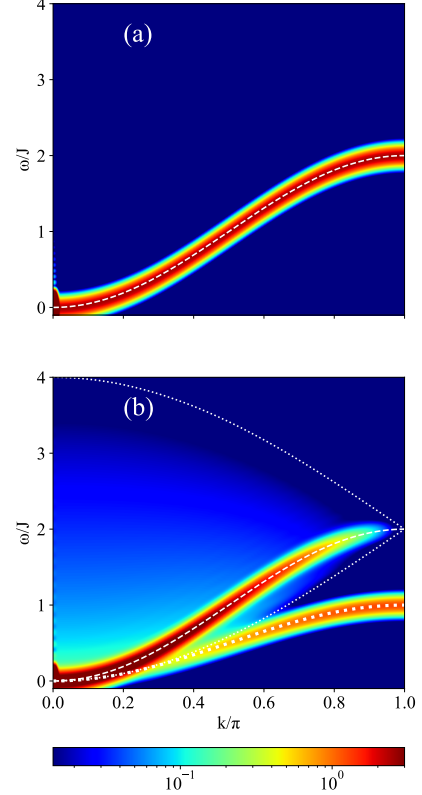


FIG. 9: Zero temperature structure factors of the one and two-spin deviation spectrum of the FM spin-1/2 chain with $J = 1$, $L = 240$ and $t_f = 40/J$. (a) $S^{-,+}(k, \omega)$, the transverse component of DSF measured in INS experiments. It only shows the spin-wave excitation (white dashed lines); (b) $S_2(k, \omega)$, the two-spin deviation spectrum. White dashed lines: single spin wave; white dotted lines: two spin-wave continuum. The bound state of spin-waves is denoted by a thick white dotted line. Note that this structure factor is not measurable in an INS experiment.

Appendix B: Thermal DSF in a magnetic field

In this Appendix, we study the problem in the presence of an external magnetic field defined by the Hamiltonian:

$$H_{FM,h} = -J \sum_i \mathbf{S}_i \cdot \mathbf{S}_{i+1} + h \sum_i S_i^z \quad (\text{B1})$$

Since single-spin-deviation states gain Zeeman energy h and two-spin-deviation states gain Zeeman energy $2h$, the dispersion relation for spin-wave and the dispersion relation for the bound state becomes.

$$\begin{aligned} \omega_{1,h}(k) &= J(1 - \cos k) + h \\ \omega_{2,BS,h}(k) &= J \sin^2 \frac{k}{2} + 2h \end{aligned}$$

The model is no longer isotropic, therefore, we have 3 different thermal DSF component namely - (i) Longitu-

dinal component $S^{z,z}(k, \omega)_\beta$, (ii) Transverse component $S^{+, -}(k, \omega)_\beta$ and (iii) Transverse component $S^{-, +}(k, \omega)_\beta$.

1. Longitudinal Dynamical Structure Factor in a magnetic field

The degeneracy of the FM ground state is lifted upon applying an external magnetic field and the ground state of Hamiltonian $\mathcal{H}_{FM,h}$ is given by the fully polarised state in the direction opposite to the magnetic field. We can evaluate the zero-temperature longitudinal component of the DSF by computing the time-dependent correlation between the z -components and then taking both spatial and temporal Fourier transform

$$C_{zz}(m, n; t) = \langle \text{GS} | S_m^z(t) S_n^z | \text{GS} \rangle$$

$$S^{zz}(k, \omega) = \frac{1}{L^2} \int_{-\infty}^{\infty} dt \sum_{m,n} C_{zz}(m, n; t) e^{-ik(r_n - r_m)} e^{-i\omega t}$$

As the groundstate is a fully polarized state in negative direction, we directly evaluate the longitudinal component of the DSF and find:

$$S^{zz}(k, \omega) = \frac{-S}{L^2} \int_{-\infty}^{\infty} dt \sum_{m,n} \langle \text{GS} | S_m^z | \text{GS} \rangle e^{-ik(r_n - r_m)} e^{-i\omega t}$$

$$= \frac{2\pi S^2}{L^2} \delta(\omega) \sum_{m,n} e^{-ik(r_n - r_m)} = \frac{\pi}{2} \delta(\omega) \delta(k) \quad (\text{B2})$$

As a result, at zero temperature, all the spectral weight is concentrated at $\omega = 0, k = 0$. Upon increasing the temperature, the spin-wave state gathers spectral weight with more weight still concentrated near $\omega, k \approx 0$. This is also true if we decrease the magnetic field for a given temperature. Since the weights near $\omega = k = 0$ are at least one order of magnitude more than the rest of the ω or k values, it is very unlikely to observe the spin-waves or bound state at finite temperature INS experiments in the longitudinal channel. We summarise the findings on longitudinal component of DSF in fig.10.

2. Transverse Dynamical Structure Factor in a magnetic field

In this section, we present the numerical results of the transverse component $S^{-, +}(k, \omega)_\beta$ where we obtain clear signature of bound state (see fig.11). We attempted a simple calculation by only keeping the most dominant terms in the thermal DSF at low temperatures - the single excitation on fully-aligned-state (denoted as $|\text{GS}\rangle$) leading to spin-wave state (denoted as $|\gamma_1\rangle$) and the excitation from a single spin-wave state to a bound state of two spin-waves (denoted as $|\alpha_{\text{BS}}\rangle$). The thermal DSF can be expressed in the Lehmann representation as:

$$S^{-, +}(k, \omega)_\beta = \frac{2\pi}{L\mathcal{Z}} \sum_{\eta, \gamma} e^{-\beta E_\gamma} |\langle \eta | S_{-k}^+ | \gamma \rangle|^2 \delta(\omega - [\omega_\eta - \omega_\gamma])$$

where \mathcal{Z} is the partition function and $|\eta\rangle$ or $|\gamma\rangle$ are eigenstates of the model. Thus, the thermal DSF becomes:

$$S^{-, +}(k, \omega)_\beta \propto \frac{e^{-\beta E_0}}{\mathcal{Z}} \left(\sum_{\gamma_1} |\langle \gamma_1 | S_{-k}^+ | \text{GS} \rangle|^2 \delta(\omega - \omega_{1,h}) + \sum_{\alpha_{\text{BS}}, \gamma_1} e^{-\beta \omega_{1,h}} |\langle \alpha_{\text{BS}} | S_{-k}^+ | \gamma_1 \rangle|^2 \delta(\omega - [\omega_{2,\text{BS},h} - \omega_{1,h}]) + \dots \right)$$

The first term inside the bracket is easily calculated:

$$\sum_{\gamma_1} |\langle \gamma_1 | S_{-k}^+ | \text{GS} \rangle|^2 \delta(\omega - \omega_{1,h}(p)) = \delta(\omega - \omega_{1,h}(k))$$

As expected the spin-wave excitation is shifted by h . It is thermally broadened in the plots (Fig. 11), but the analytical computation does not capture it here.

For the second term, since the bound state is labelled by the centre of mass momentum (K), the sum over states corresponds to a sum over K . We can determine the bound state from Eqs. A1 and A2. Since, the single spin-wave states are characterised by their momentum p , the sum over single spin wave states is replaced by a sum over momentum p . The $S^{-, +}(k, \omega)_{\beta,2}$ is thus proportional to:

$$\sum_{K,p} e^{-\beta \omega_{1,h}(p)} |\langle \alpha_{\text{BS}} | S_{-k}^+ | \gamma_1 \rangle|^2 \times$$

$$\delta(\omega - [\omega_{\text{BS},h}(K) - \omega_{1,h}(p)])$$

$$= \frac{16}{L} \sum_p e^{-\beta \omega_{1,h}(p)} \left| \sin \frac{p+k}{2} \right|^2 |f_s(p+k; p-k)|^2$$

$$\delta(\omega - [\omega_{\text{BS},h}(p+k) - \omega_{1,h}(p)])$$

where, in the thermodynamic limit ($L \gg 1$), the factor $f_s(p+k; p-k)$ is given by:

$$\frac{\cos\left(\frac{p-k}{2}\right) - \cos\left(\frac{p+k}{2}\right)}{3 + \cos(p+k) - 2\cos p - 2\cos k}$$

We can choose a section cut (at $k = \pi$) to compare our analytical results with the numerical results. We develop $S^{-, +}(k = \pi, \omega)_{\beta,2}$ in the continuum limit of the momentum of the spin-wave (p) and evaluate the integral. It is proportional to the following integral:

$$\frac{16e^{-\beta h}}{2\pi} \int_{p=-\pi}^{p=\pi} dp e^{-2\beta J \sin^2 \frac{p}{2}} \frac{\sin^2 \frac{p}{2} \cos^2 \frac{p}{2}}{(1 + 3 \sin^2 \frac{p}{2})^2} \times$$

$$\delta\left(\omega - J\left(1 - 3 \sin^2 \frac{p}{2}\right) - h\right) \quad (\text{B3})$$

We note that the integral (Eq. B3) is even about $p = 0$, so we reduce the range of p . Then upon doing a change of variable $t = \sin^2 \frac{p}{2}$, we get:

$$\frac{16e^{-\beta h}}{3\pi J} \int_0^1 dt e^{-2\beta J t} \left\{ \frac{\sqrt{t(1-t)}}{(1+3t)^2} \right\} \delta\left(t - \left(\frac{-\omega + J + h}{3J}\right)\right)$$

which, for $-2J + h \leq \omega \leq J + h$, leads to:

$$\frac{16e^{-\beta h}}{9\pi} e^{-\frac{2}{3}\beta(J+h-\omega)} \frac{\sqrt{(J+h-\omega)(2J-h+\omega)}}{(\omega - 2J - h)^2} \quad (\text{B4})$$

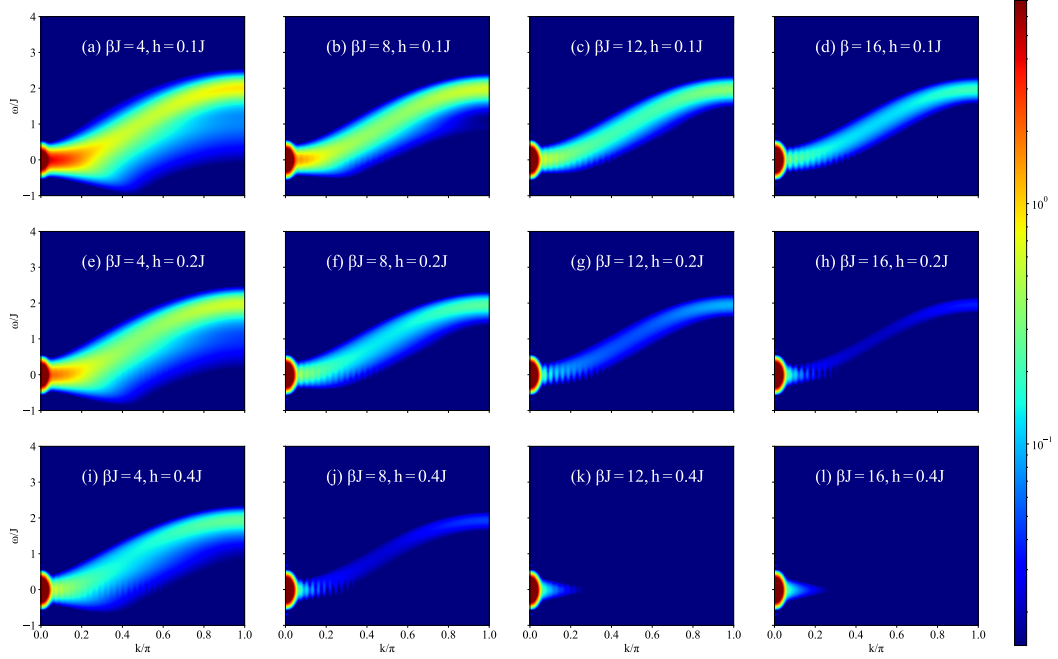


FIG. 10: Longitudinal thermal DSF($S^{zz}(k, \omega; \beta)$) of the spin-1/2 FM chain in the presence of a magnetic field, $L = 140$, $t_f = 20/J$. The spectral weight gathered by the spin-wave dispersion is one-tenth of the spectral weight at $\omega = 0, k = 0$. Signatures of the bound state are visible, but they are one-hundredth the spectral weight of the main feature.

3. Section cut in the limit of a vanishing magnetic field

In the limit of h going to 0, the system becomes isotropic and the transverse component is simply equal to two times the longitudinal component of the thermal DSF. One can determine the prefactor numerically from the free-energy density (in Fig. 1d) using the formula $F = -k_B T \ln \mathcal{Z}$. We have plotted it against the numerical thermal t-DMRG section cut (in Fig. 3a) and we find that even from this simple calculation, we can qualitatively explain the asymmetric spectral peak associated with bound state at $k = \pi$ (in Fig. 3a). One finds

that the bound state area is complicated but for very low temperatures, we can replace the free-energy density with the modified spin-wave theory free-energy density formula (Eq.5) and determine the integral numerically. Its temperature dependence is consistent with $T^{3/2}$ as shown in Fig. 3b. We plot the derivative of the log of the area under the bound state feature in the section-cut with respect to $\log T$ to find the effective exponent as a function of temperature. At very low temperature the exponent tends towards $3/2$. Note that this calculation does not include contributions from multi-spin-wave scattering states to the bound state. This is presumably why the effective exponent only tends to the expected value at very low temperatures.

-
- [1] H. Bethe, Zur theorie der metalle i. eigenwerte und eigenfunktionen der linearen atomkette, *Journal Zeitschrift für Physik* **71**, 205 (1931).
 - [2] F. Bloch, Zur theorie des ferromagnetismus, *Zeitschrift für Physik* **61**, 206 (1930).
 - [3] F. J. Dyson, General theory of spin-wave interactions, *Phys. Rev.* **102**, 1217 (1956).
 - [4] M. Wortis, Bound states of two spin waves in the heisenberg ferromagnet, *Phys. Rev.* **132**, 85 (1963).

- [5] D. C. Mattis, *The Theory of Magnetism I* (Springer, 1981).
- [6] F. D. M. Haldane, Excitation spectrum of a generalised heisenberg ferromagnetic spin chain with arbitrary spin, *Journal of Physics C: Solid State Physics* **15**, L1309 (1982).
- [7] F. D. M. Haldane, The soliton wavenumber cut-off and the excitation spectrum of the 1-d heisenberg ferromagnet in the semiclassical continuum approximation, *Jour-*

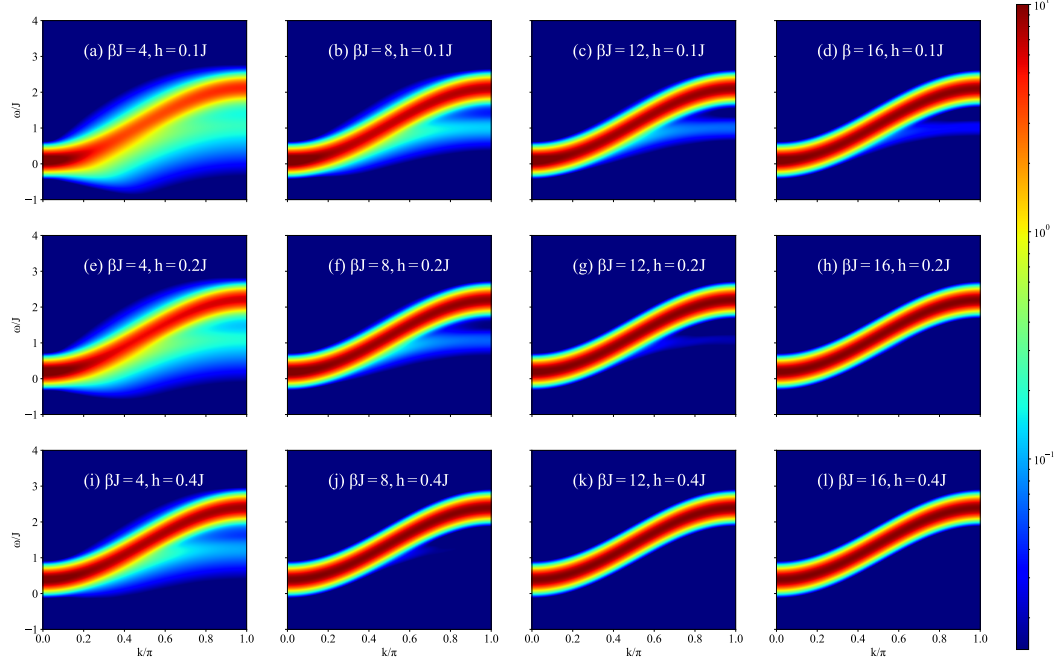


FIG. 11: Transverse thermal DSF ($S^{-,+}(k, \omega; \beta)$) of the spin-1/2 FM chain in the presence of a magnetic field, $L = 140$, $t_f = 20/J$. The spin-wave dispersion is shifted in energy by h (the strength of the magnetic field). The bound state at higher temperatures and lower magnetic fields gathers more spectral weights. It must be noted that these spectral weights are much smaller in magnitude than in the case of zero-magnetic field.

- nal of Physics C: Solid State Physics **15**, L831 (1982).
- [8] H. J. Mikeska, Solitons in a one-dimensional magnet with an easy plane, Journal of Physics C: Solid State Physics **11**, L29 (1977).
 - [9] H. G. Bohn, W. Zinn, B. Dorner, and A. Kollmar, Neutron scattering study of spin waves and exchange interactions in ferromagnetic EuS, Phys. Rev. B **22**, 5447 (1980).
 - [10] K. Kopinga, W. J. M. de Jonge, M. Steiner, G. C. de Vries, and E. Frikkee, Short- and long-range correlations in the $s=1/2$ ferromagnetic chain system ($\text{C}_6\text{D}_{11}\text{ND}_3$)CuBr₃, Phys. Rev. B **34**, 4826 (1986).
 - [11] P. Chauhan, F. Mahmood, H. J. Changlani, S. M. Koohpayeh, and N. P. Armitage, Tunable magnon interactions in a ferromagnetic spin-1 chain, Phys. Rev. Lett. **124**, 037203 (2020).
 - [12] T. Chatterjee, *Neutron Scattering from Magnetic Materials* (Elsevier, 2006).
 - [13] G. De Vries, E. Frikkee, K. Kakurai, M. Steiner, B. Dorner, K. Kopinga, and W. De Jonge, Neutron scattering study of spin waves in the $s = 1/2$ ferromagnetic chain system ($\text{C}_6\text{D}_{11}\text{ND}_3$)CuBr₃ (CHAB), Physica B: Condensed Matter **156-157**, 266 (1989).
 - [14] R. Silbergliitt and A. B. Harris, Effect of bound states on the excitation spectrum of a heisenberg ferromagnet at low temperature, Phys. Rev. Lett. **19**, 30 (1967).
 - [15] R. Silbergliitt and A. B. Harris, Dynamics of the heisenberg ferromagnet at low temperatures, Phys. Rev. **174**, 640 (1968).
 - [16] M. Date and M. Motokawa, Spin-cluster resonance in $\text{CoCl}_2 \cdot 2\text{H}_2\text{O}$, Phys. Rev. Lett. **16**, 1111 (1966).
 - [17] J. B. Torrance and M. Tinkham, Excitation of multiple-magnon bound states in $\text{CoCl}_2 \cdot 2\text{H}_2\text{O}$, Phys. Rev. **187**, 595 (1969).
 - [18] T. Barthel, U. Schollwöck, and S. R. White, Spectral functions in one-dimensional quantum systems at finite temperature using the density matrix renormalization group, Phys. Rev. B **79**, 245101 (2009).
 - [19] T. Barthel, Precise evaluation of thermal response functions by optimized density matrix renormalization group schemes, New Journal of Physics **15**, 073010 (2013).
 - [20] N. Kestlin and T. Giamarchi, Low-dimensional correlations under thermal fluctuations, Phys. Rev. B **99**, 195121 (2019).
 - [21] F. Verstraete, J. J. García-Ripoll, and J. I. Cirac, Matrix product density operators: Simulation of finite-temperature and dissipative systems, Phys. Rev. Lett. **93**, 207204 (2004).
 - [22] U. Schollwöck, The density-matrix renormalization group in the age of matrix product states, Annals of Physics **326**, 96 (2011), january 2011 Special Issue.
 - [23] S. Paeckel, T. Köhler, A. Swoboda, S. R. Manmana, U. Schollwöck, and C. Hubig, Time-evolution methods for matrix-product states, Annals of Physics **411**, 167998 (2019).
 - [24] S. R. White and A. E. Feiguin, Real-time evolution using the density matrix renormalization group, Phys. Rev.

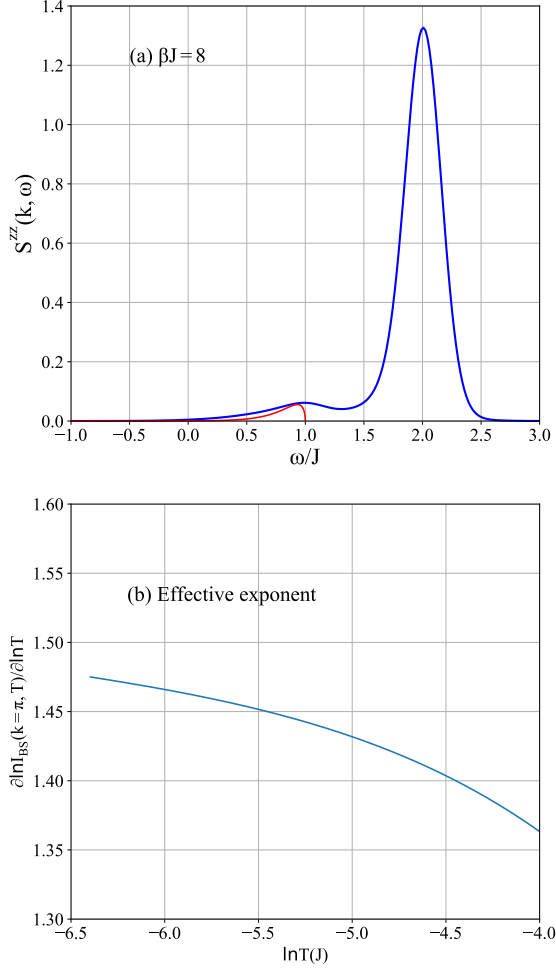


FIG. 12: a) Comparison of the numerically determined t-DMRG section cut of the spin-1/2 FM chain at $k = \pi$ (blue) and a simple estimate of the bound state thermal weight (red). The simple estimate misses spectral weight because we only included excitations with a single spin-wave state in thermal population. The effective exponent has been determined by taking the derivative of the log of the area under the curve with respect to log of the temperature.

Lett. **93**, 076401 (2004).

- [25] P. Bouillot, C. Kollath, A. M. Läuchli, M. Zvonarev, B. Thielemann, C. Rüegg, E. Orignac, R. Citro, M. Klanjšek, C. Berthier, M. Horvatić, and T. Giamarchi, Statics and dynamics of weakly coupled antiferromagnetic spin- $\frac{1}{2}$ ladders in a magnetic field, *Phys. Rev. B* **83**, 054407 (2011).
- [26] N. Fukuda and M. Wortis, Bound states in the spin wave problem, *Journal of Physics and Chemistry of Solids* **24**,

1675 (1963).

- [27] M. Takahashi, Quantum Heisenberg Ferromagnets in One and Two Dimensions at Low Temperature, *Progress of Theoretical Physics Supplement* **87**, 233 (1986).
- [28] M. Takahashi, One-Dimensional Heisenberg Model at Finite Temperature, *Progress of Theoretical Physics* **46**, 401 (1971).
- [29] F. Wang and D. P. Landau, Determining the density of states for classical statistical models: A random walk algorithm to produce a flat histogram, *Phys. Rev. E* **64**, 056101 (2001).
- [30] M. Troyer, S. Wessel, and F. Alet, Flat histogram methods for quantum systems: Algorithms to overcome tunneling problems and calculate the free energy, *Phys. Rev. Lett.* **90**, 120201 (2003).
- [31] B. Bauer, L. D. Carr, H. G. Evertz, A. Feiguin, J. Freire, S. Fuchs, L. Gamper, J. Gukelberger, E. Gull, S. Guertler, A. Hehn, R. Igarashi, S. V. Isakov, D. Koop, P. N. Ma, P. Mates, H. Matsuo, O. Parcollet, G. Pawłowski, J. D. Picon, L. Pollet, E. Santos, V. W. Scarola, U. Schollwöck, C. Silva, B. Surer, S. Todo, S. Trebst, M. Troyer, M. L. Wall, P. Werner, and S. Wessel, The ALPS project release 2.0: open source software for strongly correlated systems, *Journal of Statistical Mechanics: Theory and Experiment* **2011**, P05001 (2011).
- [32] T. Tonegawa, Two-Magnon Bound States in the Heisenberg Ferromagnet with Anisotropic Exchange and Uniaxial Anisotropy Energies, *Progress of Theoretical Physics Supplement* **46**, 61 (1970).
- [33] N. Papanicolaou, Unusual phases in quantum spin-1 systems, *Nuclear Physics B* **305**, 367 (1988).
- [34] S. R. Manmana, A. M. Läuchli, F. H. L. Essler, and F. Mila, Phase diagram and continuous pair-unbinding transition of the bilinear-biquadratic $s = 1$ heisenberg chain in a magnetic field, *Phys. Rev. B* **83**, 184433 (2011).
- [35] H. Aghahosseini and J. B. Parkinson, Two spin deviation states in a spin-1 system with heisenberg and biquadratic exchange, *Journal of Physics C: Solid State Physics* **11**, 461 (1978).
- [36] F. Mila and F.-C. Zhang, On the origin of biquadratic exchange in spin 1 chains, *The European Physical Journal B - Condensed Matter and Complex Systems* **16** (2000).
- [37] T. Inami, K. Kakurai, H. Tanaka, M. Enderle, and M. Steiner, Spin dynamics of the half-integer-spin quasi-one-dimensional heisenberg antiferromagnet CsMnI_3 , *Journal of the Physical Society of Japan* **63**, 1530 (1994).
- [38] R. J. Elliott and M. F. Thorpe, The effects of magnon-magnon interaction on the two-magnon spectra of antiferromagnets, *Journal of Physics C: Solid State Physics* **2**, 1630 (1969).
- [39] N. S. Headings, S. M. Hayden, R. Coldea, and T. G. Perring, Anomalous high-energy spin excitations in the high- T_c superconductor-parent antiferromagnet La_2CuO_4 , *Phys. Rev. Lett.* **105**, 247001 (2010).
- [40] M. Mourigal, M. Enderle, A. Klöpperpieper, J.-S. Caux, A. Stunault, and H. M. Rønnow, Fractional spinon excitations in the quantum heisenberg antiferromagnetic chain, *Nature Physics* **9**, 435 (2013).
- [41] J. Jeske, Á. Rivas, M. H. Ahmed, M. A. Martin-Delgado, and J. H. Cole, The effects of thermal and correlated noise on magnons in a quantum ferromagnet, *New Journal of Physics* **20**, 093017 (2018).

- [42] A. Keselman, L. Balents, and O. A. Starykh, Dynamical signatures of quasiparticle interactions in quantum spin chains, *Phys. Rev. Lett.* **125**, 187201 (2020).